A LOCALIZED PATTERN PHOTOBLEACHING METHOD FOR THE CONCURRENT ANALYSIS OF RAPID AND SLOW DIFFUSION PROCESSES

DENNIS E. KOPPEL
Department of Biochemistry, University of Connecticut Health Center, Farmington, Connecticut 06032

MICHAEL P. SHEETZ
Department of Physiology, University of Connecticut Health Center, Farmington, Connecticut 06032

ABSTRACT A scanning pattern photobleaching method for the analysis of lateral transport is described and discussed. Fluorescence bleaching with a localized pattern allows for the concurrent analysis of motions over two very different characteristic distances: ξ_o^{-1}, the repeat distance of the pattern, and W, the linear dimension of the illuminated region. The former motion is deduced from the decay of the modulation amplitude (of period ξ_o^{-1}) of fluorescence scans with the attenuated pattern, the latter from the recovery of the average fluorescence intensity. Such analysis should prove useful for the study of samples with a wide range of diffusion coefficients, and for the separation of effects arising from lateral diffusion and association dynamics. Theoretical analyses are presented for three related problems: (*a*) the effect of pattern localization on the decay of the modulation amplitude, (*b*) the effect of the pattern modulation on the recovery of the average local fluorescence intensity, and (*c*) the effect of a limited diffusion space (with linear dimensions of only a few pattern periods) on the decay of the modulation amplitude.

INTRODUCTION

Fluorescence photobleaching techniques have been widely applied to the study of the translational diffusion of fluorescently labeled molecules in a variety of systems: biological and model membranes (for recent reviews, see references 1 and 2), bulk solutions (3–6), polymer films (7), and cell cytoplasm (8–10). Photobleaching with a localized or nonuniform laser pulse is used to produce a nonuniform distribution of unbleached fluorophore. Subsequent illumination with an attenuated continuous-wave (CW) laser beam is used to monitor the rate and extent of fluorescence redistribution after photobleaching, and hence characterize the translational dynamics of the system.

Two basic approaches have been developed to study lateral diffusion in a planar geometry. The first of these uses focused spatially localized bleaching beams, placing primary emphasis on the analysis of distributions in real coordinate space (11, 12). The characteristic distance for diffusion is the radius of the focused laser beam. The other employs an extended periodic bleaching pattern (6, 7, 13–17), shifting the analytical emphasis to Fourier transform space. The characteristic distance, in this case, is the period of the pattern.

In the present communication, we report a combination of these approaches that allows for measurements over two very different distance scales simultaneously. This methodology should prove useful for the analysis of systems in which one has a wide range of diffusion coefficients, and for the separation of effects due to diffusion and association kinetics (18–21). A preliminary account of this work has appeared previously (22). We also report here an analysis of restricted diffusion in samples (e.g., small cells or membrane fragments) with linear dimensions of only a few periods of the bleaching pattern.

THEORY

We consider a version of the periodic pattern bleaching technique similar to the modulation detection method described by Lanni and Ware (16) and Davoust et al. (6; see also reference 22). The sample is illuminated with laser light in the form of a pattern of stripes. Pulse bleaching in this configuration produces a periodic pattern of unbleached fluorescent molecules. The modulation amplitude and phase of this concentration pattern, as well as the average concentration, is monitored as a function of time after bleaching with a series of fluorescence scans of the attenuated illumination pattern along a scan axis perpendicular to the stripes. This type of photobleaching experiment has three characteristic distances: the pattern period (ξ_o^{-1}), the linear dimensions (W and L, respectively) of the illuminated region, and the sample area to which diffusion is confined. In the following sections we analyze three useful limiting cases defined by the relative values of ξ_o^{-1}, W, and L. In the first of these, we make the usually implicit assumption that both the illumination pattern and the

sample area are unbounded, i.e., that both $\xi_o W$ and $\xi_o L$ are effectively infinite.

In the second case, bleaching is effected with a localized periodic pattern, $\xi_o L$ is effectively infinite, but $\xi_o W$ is now finite. As indicated above, this configuration can provide significant practical advantages in many situations. We conclude with an analysis of the effects of restricted diffusion, i.e., finite values of $\xi_o L$. This is a situation that one must deal with, for example, when studying diffusion on or within small cells, organelles, or membrane fragments.

Extended Pattern and Unrestricted Diffusion

We measure $F(x',t)$, the fluorescence intensity, at time t after bleaching, excited by the laser illumination pattern ($I[x, x']$) centered at position x' along the scan axis. To within a constant of proportionality.

$$F(x', t) = \int_{-\infty}^{\infty} c(x, t)\, I(x, x')\, dx, \tag{1}$$

where $c(x, t)$ is the concentration distribution of unbleached fluorophore. Specifying only that the illumination pattern is a periodic function of x with repeat distance ξ_o^{-1}, $I(x, x')$ can be written as

$$I(x, x') = \sum_{n=-\infty}^{\infty} a_n e^{2\pi i n \xi_o (x - x')}. \tag{2}$$

Combining Eqs. 1 and 2,

$$F(x', t) = \sum_{n=-\infty}^{\infty} a_n \tilde{c}\,(n\xi_o, t) e^{-2\pi i n \xi_o x'}, \tag{3}$$

where

$$\tilde{c}\,(\xi, t) \equiv \int_{-\infty}^{\infty} c(x, t) e^{2\pi i \xi x} dx, \tag{4}$$

is the Fourier transform of $c(x, t)$.

Each fluorescence scan is recorded for x' stepping over a range slightly greater than a small integral number ($m = 1$ or 2) of pattern periods. For each scan, computer analysis calculates the complex modulation amplitude

$$A(\xi_o t) \equiv \frac{\xi_o}{m} \int_{-m/2\xi_o}^{+m/2\xi_o} F(x', t) e^{2\pi i \xi_o x'} dx', \tag{5}$$

by numerical integration. Substituting $F(x', t)$ from Eq. 3 gives the simple result

$$A(\xi_o, t) = a_1 \tilde{c}(\xi_o, t), \tag{6}$$

i.e., $A(\xi_o, t)$ is proportional to the ξ_oth Fourier component of $c(x, t)$. This in turn has the usual exponential form for isotropic diffusion

$$\tilde{c}(\xi_o, t) = \tilde{c}(\xi_o, 0) e^{-(2\pi\xi_o)^2 Dt}. \tag{7}$$

We can, in addition, compute the average intensity,

$$A(0, t) \equiv \frac{\xi_o}{m} \int_{-m/2\xi_o^{-1}}^{+m/2\xi_o^{-1}} F(x', t)\, dx', \tag{8}$$

for each scan. With extended patterns, $A(0, t)$ should be constant. Normalization of $A(\xi_o, t)$ by $A(0, t)$ will correct for possible direct current (DC) drifts, such as that of fluorescence bleaching during monitoring (16).

Localized Pattern and Unrestricted Diffusion

Measurements of $A(0, t)$ now take on added importance. $A(0, t)$ recovers back towards prebleach levels as molecules diffuse over the characteristic distance W, replenishing fluorescence in the illuminated region. At the same time, the modulation amplitude, $A(\xi_o, t)$ decays as molecules diffuse over characteristic distance, ξ_o^{-1}. As we show below for even moderately large values of $\xi_o W$ the recovery of $A(0, t)$ is little affected by the presence of pattern modulation, while the decay of $A(\xi_o, t)$ is little affected by the pattern localization.

For simplicity, we consider an illumination pattern localized only relative to the scan axis. In this case, instead of Eq. 2, we now have

$$I(x, x') = P(x) \sum_{n=-\infty}^{\infty} a_n e^{2\pi i n \xi_o (x - x')}. \tag{9}$$

$P(x)$ could correspond to the image of a slit or mask in the incident beam, or the natural Gaussian profile of the laser beam itself. Combining Eqs. 1, 5, and 9, we then have

$$A(\xi_o, t) = a_1 \int_{-\infty}^{\infty} \tilde{c}(\xi, t)\, \tilde{P}\,(\xi_o - \xi)\, d\xi, \tag{10}$$

in place of Eq. 6. We can carry this one step further for general $P(x)$, if we relate $c(x, 0)$ to $I(x, x')$. In the low bleach limit (19), we have

$$c(x, 0) = 1 - \beta T I(x, 0), \tag{11}$$

where T is the bleaching time, and β is a constant that incorporates such factors as the absorption cross section and bleaching quantum efficiency of the dye. Combining Eqs. 9–11, is is shown that, to a good approximation,

$$A(\xi_o, t) - A(\xi_o, \infty) = \beta T a_1^2 \int_{-\infty}^{\infty} |\tilde{P}(\xi - \xi_o)|^2 e^{-(2\pi\xi)^2 Dt} d\xi. \tag{12}$$

Here, instead of a single exponential, as in Eqs. 6 and 7, we have a distribution of exponentials with weighting factor $|\tilde{P}(\xi - \xi_o)|^2$. The narrower the $P(x)$ in coordinate space, the broader the $|\tilde{P}(\xi - \xi_o)|^2$ in transform space.

For a more quantitative analysis, we choose a specific functional form for $P(x)$

$$P(x) = e^{-2x^2/W^2}, \tag{13}$$

the usual Gaussian profile with $1/e^2$ radius W. This, then, gives us

$$A(\xi_o, t) - A(\xi_o, \infty) \alpha (1 + 4Dt/W^2)^{-1/2} \cdot \exp\left[- \frac{(2\pi\xi_o)^2 Dt}{1 + 4Dt/W^2}\right]. \quad (14)$$

For $(\xi_o W) \gg 1$, Eq. 14 is not very different from a single exponential with decay rate $(2\pi\xi_o)^2 D$. One way to characterize the difference is through an effective diffusion coefficient calculated from the initial slope (23), i.e.,

$$D_{\text{eff}} \alpha \lim_{t \to 0} \frac{d}{dt} \ln [A(\xi_o, t) - A(\xi_o, \infty)], \quad (15)$$

with the proportionality constant chosen such that

$$\lim_{\xi_o W \to \infty} D_{\text{eff}} = D. \quad (16)$$

Combining Eqs. 14–16, we have

$$D_{\text{eff}} = D[1 + \tfrac{1}{2}(\pi\xi_o W)^{-2}]. \quad (17)$$

We can perform a similar analysis for $A(0, t)$. For general $P(x)$, in the low bleach limit, combining Eqs. 1, 8, 9, and 11,

$$A(0, \infty) - A(0, t) \simeq a_0 \beta T \int_{-\infty}^{\infty} \tilde{P}^*(\xi)[a_0 \tilde{P}(\xi) + a_{-1}\tilde{P}(\xi + \xi_0) + a_1 \tilde{P}(\xi - \xi_0)] \times e^{-(2\pi\xi)^2 Dt} d\xi. \quad (18)$$

For Gaussian $P(x)$, this reduces to

$$A(0, \infty) - A(0, t) \alpha \left\{1 - \frac{a_{-1} + a_1}{a_o} \cdot \exp\left[-\left(\pi\xi_0 W/2\right)^2 \frac{1 + 8Dt/W^2}{1 + 4Dt/W^2}\right]\right\} \times (1 + 4Dt/W^2)^{-1/2}. \quad (19)$$

Again, we can analyze the magnitude of the effect (in this case, the effect of the striped pattern on the recovery of $A[0, t]$) through calculation of an effective D. Analogous to Eq. 17, we now have

$$D_{\text{eff}} = D\left[1 + \frac{2(a_{-1} + a_1)}{a_0} e^{-(\pi\xi_0 W/2)^2}\right]. \quad (20)$$

Extended Pattern and Restricted Diffusion

We consider a sample (e.g., a cell membrane) of linear dimension L, such that fluorescently labeled molecules are free to diffuse over the range $-L/2 \le x \le L/2$, but not beyond. In a modulation amplitude analysis, in this case, Eq. 6 still holds, but Eq. 7 does not. We need a new solution to the diffusion equation with the additional boundary condition: $dc/dx = 0$ at $x = \pm L/2$, establishing the edges of the sample as impermeable to diffusion. Adapting Eq. 4.56 from reference 24, we then have

$$c(x, t) = \sum_{n=0}^{\infty} b_n \cos\left[n\pi\left(\frac{x}{L} + \frac{1}{2}\right)\right] e^{-(n\pi/L)^2 Dt}, \quad (21)$$

for $-L/2 \le x \le L/2$, and zero elsewhere, with

$$b_n = \frac{2 - \delta_{n,o}}{L} \int_{-L/2}^{L/2} c(x', 0) \cos\left[n\pi\left(\frac{x'}{L} + \frac{1}{2}\right)\right] dx', \quad (22)$$

where $\delta_{n,0}$ is the Kronecker delta function.

For simplicity, we consider an elementary form for $c(x', 0)$, namely,

$$c(x', 0) = 1 + \alpha \cos(2\pi\xi_o x'). \quad (23)$$

In this case, combining Eqs. 4, 6, 21–23, we obtain

$$A(\xi_o, t) - A(\xi_o, \infty) = \alpha a_1 \left(\frac{\sin \pi\xi_o L}{\pi\xi_o L}\right)^2 \sum_{n=1}^{\infty} [1 - (n/\xi_o L)^2]^{-2} e^{-(2\pi n/L)^2 Dt}. \quad (24)$$

As expected, $A(\xi_o, t) - A(\xi_o, \infty)$ is a sum of exponentials, with the distribution of decay rates peaking around $(2\pi\xi_o)^2 D$.

As above, we can calculate an effective value of D for this function. Combining Eqs. 15, 16, and 24, we have

$$D_{eff} = D \sum_{n=1}^{\infty} (n/\xi_o L)^2 \cdot [1 - (n/\xi_o L)^2]^{-2} / \sum_{n=1}^{\infty} [1 - (n/\xi_o L)^2]^{-2}. \quad (25)$$

This expression can be evaluated analytically. Adapting standard series expansions of trigonometric functions (Eqs. 1.422.4 and 1.423 of reference 25), we find

$$D_{\text{eff}} = D\left[1 - \frac{2 \sin(2\pi\xi_o L)}{2\pi\xi_o L + \sin(2\pi\xi_o L)}\right]. \quad (26)$$

Fig. 1 presents plots of D_{eff}/D, calculated according to Eqs. 17, 20, and 26, as functions of $\xi_o W$ or $\xi_o L$. It is seen in each case, that for even only moderately large values of $\xi_o W$ or $\xi_o L$, D_{eff} is close to D. Although these calculations incorporate a number of simplifying conditions, it is expected that the relative magnitude of the effects of finite $\xi_o W$ or $\xi_o L$ will be similar in other situations.

EXPERIMENTAL METHODS AND RESULTS

The basic optical system for the fluorescence photobleaching measurements has been described previously (12). The apparatus is centered about a modified research microscope (Ortholux II; E. Leitz, Inc., Industrial Div., Rockleigh, NJ) equipped with a fluorescence vertical illuminator. The light source for both monitoring and bleaching is a CW water-cooled argon ion laser (Laser Ionics, Orlando, FL). The input optics of the microscope perform three principal functions: forming the periodic pattern on the sample, scanning the pattern across the sample, and switching between the monitoring and bleaching intensities. A Ronchi ruling (typically 100 or 200 lines/inch; Edmund Scientific,

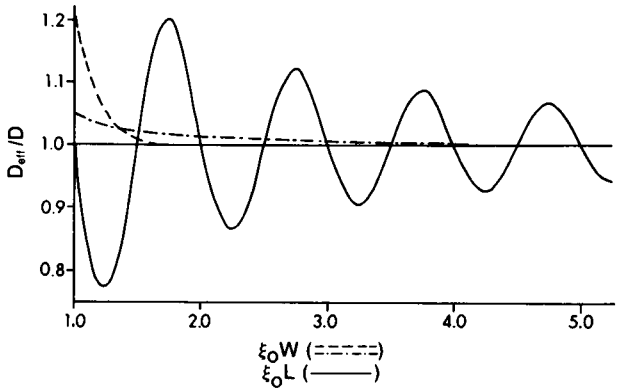

FIGURE 1 Effective values of diffusion coefficient D, demonstrating the effects of the periodic pattern on the recovery of $A(0, t)$ (---, calculated according to Eq. 20), and the effects of pattern localization (—·—, calculated according to Eq. 17) and restricted diffusion (——, calculated according to Eq. 26) on the decay of $|A(\xi_0, t)|$. In Eq. 20, a value of $(a_{-1} + a_1)/a_0 = 4/\pi$ was chosen, corresponding to a square wave illumination with an amplitude (half peak-to-peak) equal to the average intensity, a_0.

Barrington, NJ) is imaged onto the field diaphragm of the vertical illuminator (producing a well-defined localized pattern) and reimaged by the microscope optics onto the sample (13–16). Alternatively, others have used the fringe pattern formed with the interference of two coherent laser beams (6, 17), an arrangement familiar from laser Doppler velocimetry (26, 27).

A servoactivated galvanometric optical scanning mirror (model G-100PDT; General Scanning Inc., Watertown, MA) between the Ronchi ruling and the field diaphragm controls the precise angle of the incident laser beam and hence the position along a scan axis of the stripes on the sample. The outline of the field diaphragm, defining the localization of the pattern, remains stationary under these conditions. Others have scanned the Ronchi ruling itself through the incident beam (16). Alternatively, if an interference fringe pattern is employed, pattern scanning can be produced by modulating the phase of one of the incident beams (6).

The laser illumination is switched between the bleaching and the monitoring intensity (an attenuation of some 10^4-fold) by a combination of uncoated beam splitters and electronic shutters synchronized to the scanning mirror (12). Alternatively, the beam can be attenuated with neutral density filters, or an acousto-optic modulator (28). The fluorescence intensity during monitoring is detected by a thermoelectrically cooled photomultiplier tube mounted above the microscope, and quantitated with photon counting electronics synchronized to the scanning mirror.

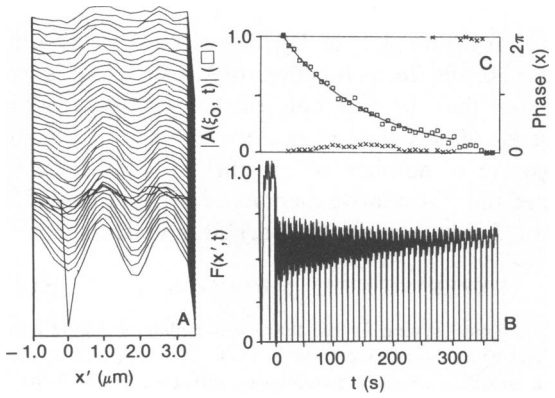

FIGURE 2 Pattern photobleaching data for a 3T3 fibroblast labeled with fluorescein-conjugated succinyl concanavalin A. (*A*) Stack of individual 24-point fluorescence scans recorded at 9.6-s intervals before and after bleaching with a pattern of stripes. (*B*) Linear sequence of the same data as recorded as a function of time. (*C*) Normalized modulation amplitude (above prebleach level) and relative phase calculated for each postbleach scan.

Fig. 2 demonstrates the capabilities of the system with data recorded on a 3T3 cell in culture labeled with fluorescein-conjugated succinyl concanavalin A (50 μg/ml for 5 min at 37°C, Vector Laboratories, Inc., Burlingame, CA). Laser illumination covered a 30-μm diam area of the cell surface with a pattern of repeat distance 1.8 μm. Fig. 2 *B* presents the entire linear sequence of data points, each corresponding to the number of fluorescence photons detected in a 300 ms counting interval. Fig. 2 *A* displays the data again, rearranged this time into a stack of individual 24-point scans recorded with 4.8-s pauses between scans. A 200-ms bleaching pulse occurs during the closed shutter point of the third scan. Subsequent scans reveal a clear periodicity as the monitoring illumination pattern is moved over the pattern of bleached fluorophore concentration.

Each scan is analyzed to give the amplitude and phase of the intensity modulation, as well as the average D.C. intensity. The average intensity is essentially constant, indicating that significant redistribution over the 15-μm characteristic distance of the illuminated region does not occur over the 10–10^3-s time scale. The modulation phase and relative modulation amplitude (above the small prebleach relative amplitude) are plotted in Fig. 2 *C*. A single exponential least-squares fit of the decay of the modulation amplitude yields a diffusion coefficient of 6.4×10^{-12} cm^2/s with (rather uncharacteristically) little evidence of an immobile component.

Fig. 3 presents preliminary data designed to examine the interactions between spectrin and actin, the principal components of the erythrocyte membrane skeleton (29, 30). Fluorescently labeled samples in 50-μm pathlength sample cells (Vitro Dynamics, Rockaway, NJ) were illuminated over an 85-μm diam. area with a pattern of repeat distance 8.5 μm. A series of 12-point scans were recorded every 4.8 s, before and after bleaching at time zero.

The top data trace (Fig. 3 *A*) is from a solution of spectrin alone, covalently labeled with dichlorotriazinylaminofluorescein (DTAF; Research Organics, Inc., Cleveland, OH) demonstrating the effects of rapid diffusion. Almost all of the bleached fluorescence intensity recovers with a characteristic time of ~35 s, corresponding to a diffusion coefficient of $\sim 1.3 \times 10^{-7}$ cm^2/s. The corresponding decay time for the modulation amplitude (which would be ~0.15 s) is too short to resolve, and indeed, no modulation above the prebleach background level is observed.

Fig. 3 *C* presents an example of the opposite extreme. The sample, in this case, is an extended aggregate of Triton extracted erythrocyte membrane skeletons (30), fluorescently labeled with DTAF. The average fluorescence intensity shows little recovery. The substantial modulation amplitude does not decay. Virtually all of the label is immobilized with diffusion coefficients $<10^{-11}$ cm^2/s. Fig. 3 *B* demonstrates an intermediate case of labeled spectrin interacting with polymerized F-actin. The observed rate and extent of fluorescence recovery and the modulation amplitude and decay rate are all intermediate between the limiting cases of Fig. 3 *A* and *C*.

DISCUSSION

A theoretical background and experimental methodology has been presented for a localized pattern photobleaching method. The redistribution after photobleaching is followed with a series of fluorescence scans of the periodic pattern (of repeat distance ξ_0^{-1}) within the bleached region (of overall radius W). Data analysis extracts three parameters from each scan.

(*a*) The average fluorescence intensity ($A[0, t]$). Redis-

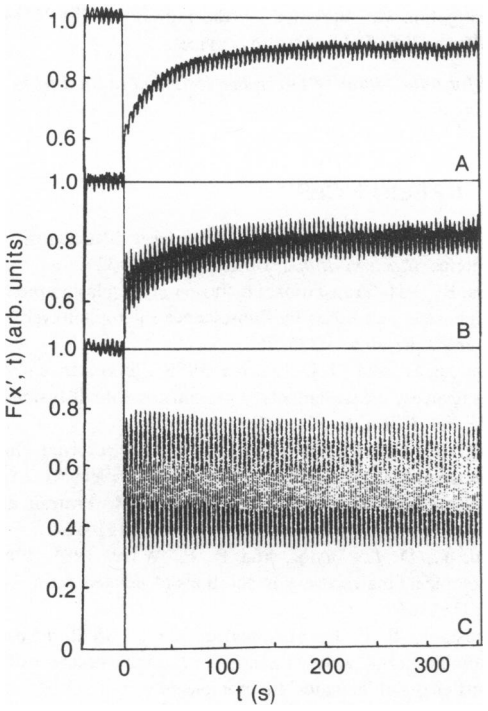

FIGURE 3 Fluorescence photobleaching data recorded with a microscope objective, manification of 25, on bulk solutions and suspensions in 50-μm pathlength flat capilliary tubes illuminated over 85-μm diam area with a pattern repeat distance of 8.5 μm. (*A*) Purified DTAF labeled spectrin dimer (0.4 mg/ml) in 0.1-M KCl, 1-mM $MgCl_2$, 5-mM imidazole buffer (pH 7.0). Human erythrocyte membranes were prepared by hypotonic lysis in 10-mM NaH_2PO_4 (pH 7.4), and were labeled by mixing (1:1) packed membranes with 1-mg/ml DTAF in 0.1-M NaH_2BO_3 (pH 9.5) for 10 min at 0°C. After washing to remove free dye spectrin was eluted and purified by the procedure of Bennett and Branton (35). (*B*) Labeled spectrin as above with, additionally, 2 mg/ml rabbit skeletal muscle actin prepared by the method of Spudich and Watt (36). (*C*) Erythrocyte membrane skeletal pellet of DTAF-labeled membranes extracted with 1% Triton X-100 in lysis buffer. *Arb. units*, arbitrary units.

tribution over the characteristic distance W produces a recovery of this intensity back toward prebleach levels. A diffusive recovery is characterized by a recovery rate

$$\Gamma_o = 4D/W^2, \tag{27}$$

which is little affected by the presence of the periodic pattern. (*b*) The modulation amplitude ($|A[\xi_o, t]|$). Redistribution over the characteristic distance ξ_o^{-1} produces a decay of this modulation back toward prebleach levels. A diffusive decay is characterized by a decay rate

$$\Gamma_1 = (2\pi\xi_o)^2 D, \tag{28}$$

which is little affected by the pattern localization. (*c*) The modulation phase. Determinations of the modulation phase define the position of the bleached pattern relative to the optic axis with remarkable precision, better than 0.05 μm in Fig. 2. Changes in this phase with time would distinguish systematic translational flow from random stochastic diffusion (31). This approach is currently being applied to study membrane flow processes associated with active cell locomotion (32–34).

The range of postbleach times for which $A(0, t)$ and $|A(\xi_o, t)|$ are determined ($t_{min} \le t \le t_{max}$) places an upper limit, Γ_{max}, and lower limit, Γ_{min}, on the accessible recovery or decay rates. Somewhat arbitrarily, we can define

$$\Gamma_{max} \simeq 1/(2t_{min}) \tag{29}$$

$$\Gamma_{max} \simeq 1/(5t_{max}). \tag{30}$$

For chosen values of W and ξ_o^{-1}, these now determine the ranges of accessible D values. This is illustrated in Fig. 4 for the parameters of Fig. 3, with $t_{min} = 4.8$ *s*, $t_{max} = 360$ s, $\xi_o^{-1} = 8.5$ μm, $W = 42.5$ μm.

The *D*-axis in Fig. 4 is divided into five distinct regions defined by the relative values of Γ_o, Γ_1, Γ_{min}, and Γ_{max}. With progressively increasing values of D these are (1) $\Gamma_o < \Gamma_1 < \Gamma_{min}$. In this case, all diffusive recovery is too slow to be observed either as a recovery of $A(0, t)$ or a decay of $|A(\xi_o, t)|$. This is the predominant case in Fig. 3 *C*. (2) $\Gamma_o < \Gamma_{min} < \Gamma_1 < \Gamma_{max}$. Diffusion over distance W is still too slow to observe, but $|A(\xi_o, t)|$ does decay over the time scale of the experiment. This is the predominant case in Fig. 2. (3) Depending upon the relative sizes of ($\Gamma_{max}/\Gamma_{min}$) and ($\Gamma_1/\Gamma_o$) there are two possibilities. (*a*) $\Gamma_{min} < \Gamma_o < \Gamma_1 < \Gamma_{max}$. Diffusive recovery is observable as both a recovery of $A(0, t)$ and a decay of $|A(\xi_o, t)|$. This is possible if ($\Gamma_{max}/\Gamma_{min}$) > Γ_1/Γ_o, i.e., from Eqs. 27–30 if $t_{max}/t_{min} > 4\,(\xi_o W)^2$. (*b*) $\Gamma_o < \Gamma_{min} < \Gamma_{max} < \Gamma_1$. Diffusive recovery is too slow to be observed as a recovery of $A(0, t)$, but so fast that a modulation amplitude is not seen. For the parameters of Fig. 4, this is possible for $D \simeq 2 \times 10^{-9}$ cm^2/s. A fluorescent component with this diffusion coefficient would appear as a decrease in the initial modulation amplitude below that otherwise expected. (4) $\Gamma_{min} < \Gamma_o < \Gamma_{max} < \Gamma_1$. Diffusive recovery is still so fast that a modulation ampli-

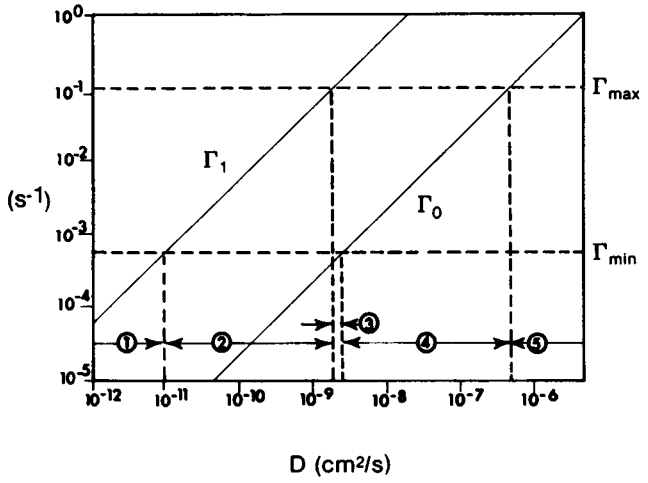

FIGURE 4 Ranges of accessible values of D calculated according to Eqs. 27–30 for the experimental parameters of Fig. 3 ($t_{min} = 4.8$ s, $t_{max} = 360$ s, $\xi_o^{-1} = 8.5$ μm, $W = 42.5$ μm). The encircled numbers correspond to the five domains discussed in the text.

tude is not seen, but can now be observed as a recovery of $A(0, t)$. This is the predominant case in Fig. 3 *A*. (5) $\Gamma_{max} < \Gamma_o < \Gamma_1$. Diffusive recovery is now so fast that even the recovery of $A(0, t)$ occurs largely before the earliest observation. The sample appears to be extraordinarily resistant to bleaching.

Fluorescence photobleaching can be applied to the study of association dynamics (18–21). The nature of fluorescence redistribution, in this case, is governed by the ratio (R) of the association reaction rate to the characteristic diffusion rate over the appropriate characteristic distance (18–21). In the diffusion limit ($R \gg 1$) each molecule switches between the bound and free states many times before diffusing over the characteristic distance. One observes a mondisperse diffusive recovery dynamically averaged over the bound and free states. In the reaction limit ($R \ll 1$), in contrast, exchange is relatively slow. One observes a statically averaged polydisperse recovery. Complete analysis requires a systematic variation of R. The concurrent analysis of motions over two very different characteristic distances makes the localized pattern photobleaching method especially attractive in this situation. One has two effective values of R (R_0 and R_1) corresponding to redistributions over characteristic distances W and ξ_o^{-1}, respectively, so that

$$\frac{R_0}{R_1} = \frac{\Gamma_1}{\Gamma_0}. \tag{31}$$

The absolute values of R_0 and R_1 define five limiting cases. For a given reaction rate, with progressively decreasing values of W and ξ_o^{-1} (keeping R_0/R_1 constant) these are (1) $R_0 \gg R_1 \gg 1$; the characteristic distances are sufficiently large that the diffusion limit applies in all cases. One observes a monodisperse recovery of $A(0, t)$ and a monodisperse decay of $|A(\xi_o, t)|$. (2) $R_0 \gg R_1 \simeq 1$. Recovery over characteristic distance W is still at the diffusion limit. Over distance ξ_o^{-1}, however, the diffusion rate is now comparable to the reaction rate. The decay of $|A(\xi_o, t)|$ is a complex function of reaction and diffusion kinetics. (3) $R_o \gg 1 \gg R_1$. For sufficiently large values of (R_0/R_1), it is possible to have $|A(\xi_o, t)|$ decay now in the reaction limit, while the recovery of $A(0, t)$ is still in the diffusion limit. (4) $R_0 \simeq 1 \gg R_1$. W is now sufficiently small that the corresponding diffusion rate is comparable to the reaction rate. The decay of $|A(\xi_o, t)|$ remains in the reaction limit. (5) $1 \gg R_0 \gg R_1$; both characteristic distances are now sufficiently small that the reaction limit applies in all cases. The data in Fig. 2 *B* appear to fall somewhere between categories 4 and 5. This type of analysis can be applied most readily to the study of ligand binding to polymer networks in bulk solution (as in Fig. 2). Under favorable circumstances, it is expected that this approach can be extended to individual cell plasma membranes, where it is believed that similar reactions affect the lateral mobility of integral membrane proteins.

This investigation was supported by research grants GM 23585 and GM 28250 from the U.S. Public Health Services.

Received for publication 14 December 1982 and in final form 28 March 1983.

REFERENCES

1. Cherry, R. J. 1979. Rotational and lateral diffusion of membrane proteins. *Biochim. Biophys. Acta.* 559:289–327.
2. Peters, R. 1981. Translational diffusion in the plasma membranes of single cells as studied by fluorescence microphotolysis. *Cell Biol. Internat. Reports.* 5:733–760.
3. Barisas, B. G., and M. D. Leuther. 1979. Fluorescence photobleaching recovery measurements of protein absolute diffusion constants. *Biophys. Chem.* 10:221–229.
4. Rigler, R., and P. Grasselli. 1980. Time resolved fluorescence spectroscopy and diffusion of biological molecules. *In* Lasers in Biology and Medicine. F. Hillenkamp, R. Pratesi, and C. A. Sacchi, editors. Plenum Press, New York. 151–164.
5. Lanni, F., D. L. Taylor, and B. R. Ware. 1981. Fluorescence photobleaching recovery in solutions of labeled actin. *Biophys. J.* 35:351–364.
6. Davoust, J., P. F. Devaux, and L. Leger. 1982. Fringe pattern photobleaching, a new method for the measurement of transport coefficients of biological macromolecules. *EMBO (Eur. Mol. Biol. Organ.) J.* 1:1233–1238.
7. Smith, B. A. 1982. Measurement of diffusion in polymer films by fluorescence redistribution after pattern photobleaching. *Macromolecules.* 15:469–472.
8. Wojcieszyn, J. W., R. A. Schlegel, E-S. Wu, and K. A. Jacobson. 1981. Diffusion of injected macromolecules within the cytoplasm of living cells. *Proc. Natl. Acad. Sci. U.S.A.* 78:4407–4410.
9. Kreis, T. E., B. Geiger, and J. Schlessinger. 1982. Mobility of microinjected rhodamine actin within living chicken gizzard cells determined by fluorescence photobleaching recovery. *Cell.* 29:835–845.
10. Wang, Y-L., F. Lanni, P. L. McNeil, B. R. Ware, and D. L. Taylor. 1982. Mobility of cytoplasmic and membrane-associated actin in living cells. *Proc. Natl. Acad. Sci. U.S.A.* 79:4660–4664.
11. Axelrod, D., D. E. Koppel, J. Schlessinger, E. L. Elson, and W. W. Webb. 1976. Mobility measurement by analysis of fluorescence photobleaching recovery kinetics. *Biophys. J.* 16:1055–1069.
12. Koppel, D. E. 1979. Fluorescence redistribution after photobleaching—A new multipoint analysis of membrane translational dynamics. *Biophys. J.* 28:281–291.
13. Smith, B. A., and H. M. McConnell. 1978. Determination of molecular motion in membranes using periodic pattern photobleaching. *Proc. Natl. Acad. Sci. U.S.A.* 75:2759–2763.
14. Smith, L. M., J. W. Parce, B. A. Smith, and H. M. McConnell. 1979. Antibodies bound to lipid haptens in model membranes diffuse as rapidly as the lipids themselves. *Proc. Natl. Acad. Sci. U.S.A.* 76:4177–4179.
15. Smith, B. A., W. R. Clark, and H. M. McConnell. 1979. Anisotropic molecular motion on cell surface. *Proc. Natl. Acad. Sci. U.S.A.* 76:5641–5644.
16. Lanni, F., and B. R. Ware. 1982. Modulation detection of fluorescence photobleaching recovery. *Rev. Sci. Instrum.* 53:905–908.
17. Weis, R. M., K. Balakrishnan, B. A. Smith, and H. M. McConnell. 1982. Stimulation of fluorescence in a small contact region between rat basophil leukemia cells and planar lipid membrane targets by coherent evanescent radiation. *J. Biol. Chem.* 257:6440–6445.
18. Koppel, D. E. 1981. Association dynamics and lateral transport in biological membranes. *J. Supramol. Struct. Cell. Biochem.* 17:61–67.

19. Elson, E. L., J. Schlessinger, D. E. Koppel, D. Axelrod, and W. W. Webb. 1976. Measurement of lateral transport on cell surfaces. *In* Membranes and Neoplasia: New Approaches and Strategies. V. T. Marchesi, editor. Alan R. Liss, Inc., New York. 137–147.
20. Thompson, N. L., T. P. Burghardt, and D. Axelrod. 1981. Measuring surface dynamics of biomolecules by total internal reflection fluorescence with photobleaching recovery or correlation spectroscopy. *Biophys. J.* 33:435–454.
21. Elson, E. L., and J. A. Reidler. 1979. Analysis of cell surface interactions by measurements of lateral mobility. *J. Supramol. Struct.* 12:481–489.
22. Koppel, D. E. 1983. Fluorescence techniques for the study of biological motion. *In* The Application of Laser Light Scattering to the Study of Biological Motion. J.C. Earnshaw and M.W. Steer, editors. Plenum Press, New York. 245–273.
23. Axelrod, D., P. Ravdin, D. E. Koppel, J. Schlessinger, W. W. Webb, E. L. Elson, and T. R. Podleski. 1976. Lateral motion of fluorescently labeled acetylcholine receptors in membranes of developing muscle fibers. *Proc. Natl. Acad. Sci. U.S.A.* 73:4594–4597.
24. Crank, J. 1956. The Mathematics of Diffusion. Oxford University Press, London. 58–60.
25. Gradshteyn, I. S., and I. M. Ryshik. 1980. Table of Integrals, Series and Products. A. Jeffrey, editor. Academic Press, Inc., New York. 36–37.
26. Pike, E. R. 1977. Photon correlation velocimetry. *In* Photon Correlation Spectroscopy and Velocimetry. H. Z. Cummins and E. R. Pike, editors. Plenum Press, New York. 246–343.
27. Born, G. V. R., A. Melling, and J. H. Whitelaw. 1978. Laser Doppler microscope for blood velocity measurements. *Biorheology.* 15:163–172.
28. Garland, P. 1981. Fluorescence photobleaching recovery: control of laser intensities with an acousto-optic modulator. *Biophys. J.* 33:481–482.
29. Lux, S. E. 1979. Dissecting the red cell membrane skeleton. *Nature (Lond.).* 281:426–429.
30. Sheetz, M. P., and D. Sawyer. 1978. Triton shells of intact erythrocytes. *J. Supermol. Struct.* 8:399–412.
31. Koppel, D. E., J. M. Oliver, and R. D. Berlin. 1982. Surface functions during mitosis III. Quantitative analysis of ligand-receptor movement into the cleavage furrow: diffusion vs. flow. *J. Cell Biol.* 93:950–960.
32. Harris, A. K. 1973. Cell surface movements related to cell locomotion. *CIBA Found. Symp.* 14:3–20.
33. Roberts, T. M., and S. Ward. 1982. Centripetal flow of pseudopodial surface components could propel the amoeboid movement of *Caenorhabditis elegans* spermatozoa. *J. Cell Biol.* 92:132–138.
34. Koppel, D. E. 1982. Measurement of membrane protein lateral mobility. *In* Techniques in the Life Sciences, B4/II. Lipid and Membrane Biochemistry. T. R. Hesketh, H. L. Kornberg, J. C. Metcalfe, D. H. Northcote, C. I. Pogson, and K. F. Tipton, editors. Elsevier Biomedical Press, County Clare, Ireland. pp. B425–1–25.
35. Bennett, V., and D. Branton. 1977. Selective association of spectrin with the cytoplasmic surface of human erythrocyte plasma membranes. Quantitative determination with purified [^{32}P] spectrin. *J. Biol. Chem.* 252:2753–2763.
36. Spudich, J. A., and S. Watt. 1971. The regulation of rabbit skeletal muscle contraction. I. Biochemical studies of the interaction of the tropomyosin-troponin complex with actin and the proteolytic fragments of myosin. *J. Biol. Chem.* 246:4866–4871.